**International Journal of Innovative Research and Reviews**, 10(1) 29-44

**International Journal of Innovative Research and Reviews**
ISSN: 2636-8919
*Website: www.injirr.com*



RESEARCH ARTICLE

# Machine Learning-Assisted Pool Boiling Parameter Prediction

Doğan ÇİLOĞLU[1,*], Mısra YILMAZ[1]

[1] *Department of Mechanical Engineering, Faculty of Engineering, Ataturk University, Erzurum, Türkiye*

** Corresponding author E-mail: dciloglu@atauni.edu.tr*

ARTICLE INFO

Received : 04.05.2026
Accepted : 06.26.2026
Published : 07.15.2026

***Keywords***:
*Boiling heat transfer coefficient*
*Critical heat flux*
*Machine learning*
*Support vector regression*
*Gradient boosting*

ABSTRACT

In this study, the pool boiling behavior of n-pentane fluid on different metallic surfaces was investigated using experimental and machine learning-based approaches. Copper, aluminum, and stainless-steel substrates were used in the experimental studies; for each surface, the uncoated condition and three different nickel coating concentrations were evaluated. Surface characterization included measurements of average surface roughness and contact angle; boiling performance was analyzed using surface superheat, heat flux, heat transfer coefficient (h), onset of nucleate boiling (ONB), and critical heat flux (CHF) parameters. Experimental results showed that nickel-coated surfaces generally reduced the onset of nucleate boiling, allowed the same heat flux to be achieved at lower surface superheat, and improved the CHF behavior, especially on aluminum and copper surfaces. Changes in surface roughness and contact angle were found to have significant effects on boiling performance. Random Forest, Gradient Boosting, and Support Vector Regression (SVR) models were developed to estimate heat flux and heat transfer coefficient using an experimental dataset. In the revised model structure, $\Delta T$, material type, surface type, nickel concentration, Ra, and contact angle were used as machine learning inputs, while pressure and saturation temperature were treated only as fixed experimental conditions. For heat transfer coefficient prediction, the primary model was reconstructed without $q''$ as an input variable to reduce direct information leakage from the defining relation $h = q''/\Delta T$. The $q''$-included h model was retained only as a secondary consistency case. Model performance was evaluated using $R^2$, RMSE, MAE, and MAPE metrics. The results showed that the SVR model provided the most successful performance in estimating h, while the Gradient Boosting model provided higher accuracy in estimating heat flux. Furthermore, the risk of overly optimistic performance, which might arise from including experimental points of the same surface in both training and test sets, was reduced by using a group-based cross-validation approach. This study evaluates the coating-material-boiling performance relationship in n-pentane pool boiling within an experimental and AI-supported framework by integrating surface characterization parameters with data-based modeling.

**Contents**

1. Introduction ..... 30
2. Materials and Methods ..... 31
2.1. Experimental origin, test matrix, and working fluid ..... 31
2.2. Surface preparation ..... 32
2.3. Experimental setup and procedure ..... 32
2.4. Data reduction and uncertainty analysis ..... 32
2.5. Surface characterization and descriptor variables ..... 33
2.6. Dataset size, group structure and representativeness ..... 33
2.7. Determination of ONB and operational CHF points ..... 33

*Cite this article* Çiloğlu D, Yılmaz M. Machine Learning-Assisted Pool Boiling Parameter Prediction. *International Journal of Innovative Research and Reviews (INJIRR)* (2026) 10(1) 29-44
*Link to this article:* http://www.injirr.com/article/view/262

Copyright © 2026 Authors.
This is an open access article distributed under the Creative Commons Attribution-NonCommercial-NoDerivatives 4.0 International License, which permits unrestricted use, and sharing of this material in any medium, provided the original work is not modified or used for commercial purposes.

2.8. Data preprocessing and outlier checking ..... 34
2.9. Model inputs, target variables, and regression algorithms ..... 34
2.10. Model validation, error metrics, and evaluation of prediction performance ..... 35
2.11. Comparison, residual analysis, and model interpretability ..... 36
2.12. Methodological rationale and scope of the selected approach ..... 36
3. Results and Discussion ..... 36
3.1. Data preprocessing and the general relationship structure between variables ..... 37
3.2. Boiling curves and critical heat flux behavior ..... 37
3.3. Heat transfer coefficient curves ..... 38
3.4. Ni concentration, ONB and boiling onset ..... 39
3.5. Surface roughness and wettability effects ..... 39
3.6. Comparative evaluation of artificial intelligence models ..... 40
3.7. Prediction accuracy and residual analysis ..... 41
3.8. Feature importance and physical interpretation ..... 42
3.9. Compatibility with literature and original contribution ..... 43
3.10. Comparative general assessment ..... 43
4. Conclusion ..... 44
Conflict of Interest ..... 44
References ..... 44

## 1. Introduction

Boiling heat transfer is a fundamental heat transfer mechanism for energy systems, electronic cooling, power generation, chemical processes, heat exchangers, and phase-change thermal management applications, as it allows for the removal of high heat fluxes with relatively small temperature differences. Pool boiling is one of the most basic boiling configurations, where a fluid undergoes a phase change over a heated surface without the effect of forced flow. Therefore, it constitutes a broad research area in the literature due to both its experimentally verifiable nature and its fundamental role in explaining the physics of boiling. However, the pool boiling process is not solely dependent on fluid properties; it is determined by the simultaneous influence of numerous parameters such as surface material, surface roughness, wettability, micro/nanostructure, coating morphology, operating pressure, and surface superheating. This multi-parameter structure makes it difficult to reliably explain and predict performance indicators, particularly the onset of nucleate boiling (ONB), heat transfer coefficient (h), and critical heat flux (CHF).

Three key quantities stand out in evaluating pool boiling behavior: ONB, h, and CHF. ONB represents the threshold at which stable bubble formation begins on the surface, while h represents the ratio of heat flux transferred from the surface to the fluid to surface superheating. CHF indicates the sustainable upper limit of the nucleate boiling regime, and exceeding this value can lead to boiling crisis, vapor shroud formation on the surface, and sudden temperature increase. Therefore, accurate determination and prediction of CHF are critical not only for performance but also for system safety. Although numerous theoretical, empirical, and data-based approaches to CHF prediction have been developed in the literature, most traditional correlations have been validated within limited ranges of fluid, surface, and operating conditions; this limits their generalizability for different surface coatings and different substrate materials [1].

Surface modification is one of the most commonly used methods to improve pool boiling performance. Micro/nano-scale structured surfaces, rough surfaces, porous coatings, and modified wettability surfaces can increase bubble nucleation sites, facilitate liquid feeding, and alter the dynamics of vapor bubble separation from the surface. Current review studies highlight that the improvement in boiling performance occurs mostly through three main mechanisms: regulation of nucleation site density and bubble dynamics, enhancement of capillary liquid feeding, and enhancement of the heat transfer area with multi-scale/hybrid surface architectures [2]. In this context, metallic surface modifications such as nickel plating have the potential to improve pool boiling performance as they can alter both surface topography and wettability.

In pool boiling, the effects of surface roughness and wettability on h and CHF have long been studied by researchers. It is generally accepted that roughness can improve heat transfer in the nucleate boiling regime by increasing active nucleation sites, while wettability has a particularly strong effect on CHF behavior. However, these effects are not always unidirectional and linear. Excessive roughness can negatively impact heat transfer, such as when porous structures cause vapor trapping or the coating restricts liquid supply paths. Similarly, a decrease in contact angle can improve CHF by increasing liquid diffusion, but it can also alter nucleation ease and bubble separation characteristics. Therefore, the combined effects of surface roughness, contact angle, and material need to be considered.

Experimental studies on n-pentane have shown that micro/nano-structured surfaces alter the boiling heat transfer coefficient and CHF behavior. In the study conducted by Liu et al. on n-pentane, flat and micro/nano-structured surfaces were compared; the effects of surface structure on h and CHF were evaluated [3]. However, it has also been reported that the effect of surface modification on CHF in n-pentane and similar low boiling point fluids is not always in the same direction. However, the effect of surface modification on CHF is not always unidirectional. The increase in CHF depends not only on the increase in roughness but also on the combined effect of wettability, capillary fluid supply, surface morphology, and fluid rewetting capability. O'Hanley et al. [4], by examining the separate effects of surface roughness, wettability, and porosity on CHF, showed that the CHF behavior in improved surfaces should be explained by

multiple surface parameters. This shows that the "coating on/off" approach alone is insufficient; This indicates that coating concentration, roughness, contact angle, substrate material, and heat flux regime must be analyzed together.

A significant portion of the literature on surface modification focuses on fluids such as water, FC-72, HFE, or acetone. Studies on n-pentane are more limited, and there are relatively few studies that compare different metallic substrates within the same methodological framework, evaluating nickel plating concentration and surface characterization parameters together. Furthermore, while many experimental studies present boiling curves and CHF values, they do not systematically compare experimental results with data-based models that predict the obtained data. This creates a significant gap in terms of transforming experimental observations into a more generalizable predictive structure.

In recent years, machine learning approaches have been increasingly used in boiling heat transfer and CHF estimation studies. Current reviews on CHF estimation show a clear trend from empirical correlations to numerical models and machine learning-based approaches [5]. The main reason for this trend is that quantities such as CHF and HTC are determined by the nonlinear interaction of numerous physical parameters. Models such as Random Forest, Gradient Boosting, support vector regression, and artificial neural networks have the potential to capture multivariate and nonlinear relationships where classical correlations are limited. However, evaluating machine learning models solely on the basis of statistical accuracy is not sufficient; the physical significance of the model inputs, a validation strategy appropriate to the experimental data structure, and the preservation of physical boundary points such as ONB/CHF are also important for methodological reliability.

Three main research gaps stand out in the current literature. First, there are limited studies that comparatively address different metallic substrates and nickel-plating concentrations in n-pentane pool boiling within the same data structure. Secondly, it is not sufficiently common to include characterization parameters such as surface roughness and contact angle (θ) along with heat flux (q"), h, ONB, and CHF results in a data-driven modeling framework. Thirdly, the use of validation approaches that consider surface groups instead of random data splitting in machine learning-based predictions is still limited. However, experimental points belonging to the same surface are not independent of each other; therefore, random splitting can make model performance appear higher than it actually is. The group-based validation approach used in this study aims to reduce this methodological weakness.

In this study, the pool boiling behavior of n-pentane fluid on copper, aluminum, and stainless-steel surfaces were investigated using experimental data and a machine learning-supported prediction approach. For each substrate material, an uncoated surface and three different nickel coating concentrations were evaluated; thus, the effects of coating concentration, surface roughness, contact angle, and substrate material were analyzed together. The experimental dataset was structured to include surface superheat (ΔT), q", h, ONB, and CHF information. In terms of modeling, q" and h were considered as two separate target variables; Random Forest, Gradient Boosting, and support vector regression models were compared.

The main objective of this study is not only to present experimental boiling curves, but also to relate the behaviors obtained from these curves to surface characterization parameters and to evaluate the predictability of experimental results. ΔT, material type, surface type, Ni concentration, surface roughness, and contact angle were used as the main model inputs. Pressure and saturation temperature were not used as machine learning inputs because they remained constant throughout the experiments. For heat transfer coefficient estimation, the primary model was reconstructed without q″ as an input variable to reduce direct information leakage from the defining relation h = q″/ΔT. The q″-included h model was retained only as a secondary consistency case. Model performance ($R^2$) was evaluated using RMSE, MAE, and MAPE metrics; empirical-predictive comparisons were supported by residual analyses and permutation significance analyses.

The unique value of this study can be summarized in four main points. First, three different metallic substrates and different nickel-plating concentrations for a low boiling point fluid like n-pentane were evaluated within the same methodological framework. Second, the study was not limited to comparing only boiling curves and CHF values; surface characterization parameters such as mean surface roughness (Ra), contact angle (θ), and nickel concentration were included in the data-based prediction model. Third, physically critical points such as ONB and CHF were algorithmically marked and preserved during the outlier removal process. This approach prevented the data removal process from distorting the boiling physics. Fourth, group-based cross-validation was used in model validation; thus, the risk of overly optimistic performance that might arise from the presence of experimental points of the same surface in both the training and test sets was reduced.

In these respects, this study combines classical experimental pool boiling analysis with machine learning-supported prediction and interpretability tools. Although it has been widely shown in the literature that surface modifications can improve pool boiling performance, it is known that this effect can vary depending on fluid, surface chemistry, roughness, wettability and substrate material [6] Therefore, the contribution of the present study is to evaluate the effects of nickel-plated surfaces on n-pentane pool boiling not only at the experimental observation level but also in terms of predictability, error structure and variable importance ranking. Thus, the study offers an integrated experimental and data-based framework to explain the coating-material-surface property interaction in n-pentane pool boiling.

## 2. Materials and Methods

### 2.1. Experimental origin, test matrix, and working fluid

The experimental dataset used in the present machine learning-assisted study was generated from the authors' saturated pool boiling experiments, rather than being collected from an external open literature database. The experiments were conducted using n-pentane as the working

fluid on three different metallic substrates: copper (Cu), AISI 304 stainless steel (SS), and aluminum (Al 6061). For each substrate, one uncoated surface and three electrochemically Ni-coated surfaces were evaluated, resulting in a total of twelve material–surface groups.

The coating conditions were defined as bare surface, K1, K2, and K3. In the machine learning dataset, these conditions were represented by Ni concentration values of 0 M for the bare surface and 1.607 M, 2.716 M, and 4.35 M for the coated surfaces, respectively. The experiments were conducted under the local atmospheric pressure of approximately 0.83 bar, corresponding to a saturation temperature of approximately 29 °C for n-pentane. Since all experiments were performed at the same pressure and saturation temperature, these two parameters were used only to define the experimental condition and calculate wall superheat; they were not retained as informative machine learning input variables in the revised model structure.

In the pool boiling literature, surface roughness, micro/nano structure, contact angle, and coating morphology are widely reported to be decisive factors in ONB, HTC, and CHF. In particular, micro/nano-structured surface studies with n-pentane have reported that structured surfaces increase the heat transfer coefficient and reduce surface overheating at the CHF point; this effect is associated with increased nucleation site density, expanded heat transfer area, and improved liquid diffusion [3]. Therefore, the inclusion of Ra, θ, coating concentration, and material type together in the model in the present study offers a modeling approach that is justifiable not only statistically but also physically.

## 2.2. Surface preparation

Before the boiling experiments, the flat test surfaces were mechanically polished using P1200 sandpaper and finished with alumina. To increase the active surface area, the surfaces were chemically etched using hot aqua regia prepared from HCl, $HNO_3$, and distilled water. After etching, the specimens were cleaned with alcohol to remove organic residues and rinsed with distilled water.

The electrochemical coating process was carried out in two stages. First, a thin Cu interlayer was deposited on the test surface to improve the adhesion of the subsequent Ni coating to the base substrate. During this step, a copper electrode was used as the dissolving anode, and the Cu coating was performed in an acidic $CuSO_4$–$H_2SO_4$ bath. The bath pH was adjusted to approximately 2–3, and the coating process was conducted at 30–40 °C under continuous magnetic stirring. The non-boiling surfaces of the specimens were masked with epoxy-based paint so that the electrochemical reaction occurred only on the active heating surface.

In the second stage, Ni coating was deposited electrochemically on the Cu-interlayered specimens. A cleaned Ni plate was used as the anode, while the Cu, SS, and Al specimens were used as cathodes. The Ni coating bath was maintained at 35 °C and stirred at 250 rpm. The coating time was 15 min for all specimens, while the applied currents were 0.8 A, 2 A, and 1 A for Cu, SS, and Al substrates, respectively. Three different electrolyte compositions were used to obtain the K1, K2, and K3 coating conditions (Table 1).

Table 1 Electrolyte compositions used for Ni coating.

| Coating condition | NiCl2 (g/L) | NiSO4 (g/L) | H3BO3 (g/L) | Total Ni-solution concentration used in ML dataset (Molar) |
|---|---|---|---|---|
| K1 | 50 | 250 | 40 | 1.607 |
| K2 | 75 | 375 | 60 | 2.716 |
| K3 | 100 | 500 | 80 | 4.35 |

## 2.3. Experimental setup and procedure

The pool boiling experiments were conducted in a facility consisting mainly of a boiling chamber, condenser, heater, power supply, data acquisition unit, and temperature measurement system. The boiling chamber was fabricated from Pyrex glass with a diameter of 100 mm and a height of 200 mm. A condenser was installed on the chamber lid to condense the vapor generated during boiling and to maintain the liquid level during the experiments.

The test specimen was mounted at the bottom of the boiling chamber in a leak-tight manner. Heat was supplied from below using a 2.5 kW heater, which was insulated with rock wool to direct the generated heat toward the test surface. The system was powered by a 5 kW AC power supply. Three K-type thermocouples were positioned beneath the test specimen to measure the heating surface temperature. The surface temperature was obtained from the average of these thermocouples, and the small temperature drop over the 2 mm distance between the thermocouple locations and the boiling surface was estimated using Fourier's law. A separate vertical K-type thermocouple was used to measure the fluid temperature in the boiling chamber. All thermocouples were calibrated using a water bath, and temperature–time data were recorded using LabVIEW through a National Instruments NI cDAQ-9178 data acquisition card.

Each experiment was performed using approximately 400 mL of n-pentane. At the beginning of the test, the input power was adjusted to reach a heat flux of approximately 8.5 kW/m² and to bring the fluid to saturation. At each power step, a waiting period of approximately 10 min was applied to establish thermal equilibrium between the heating surface and the fluid. After steady conditions were reached, the heat flux was increased gradually by 5%. Near the CHF region, the power increment was reduced first to 3% and then to 2% to capture the limiting heat flux more carefully. When a vapor layer formed on the surface and a rapid increase in surface temperature was observed, the power supply was immediately cut off and the test was terminated.

## 2.4. Data reduction and uncertainty analysis

The wall superheat was calculated as the difference between the heating surface temperature and the saturation temperature of n-pentane:

$$\Delta T = T_s - T_{sat} \quad (1)$$

where Ts is the heating surface temperature and $T_{sat}$ is the saturation temperature of n-pentane at the local experimental pressure.

The active boiling surface was circular with a diameter of 40 mm, corresponding to an effective heat transfer area of 12.56

cm². The heat flux supplied to the boiling surface was calculated from the measured voltage and current as:

$$q'' = VI/A \quad (2)$$

where V is the applied voltage, I is the current, and A is the effective heat transfer area.

The pool boiling heat transfer coefficient was calculated as:

$$h = q''/(T_s - T_{sat}) = q''/\Delta T \quad (3)$$

Uncertainty analysis was performed according to the Kline–McClintock method to quantify the propagation of measurement errors into the calculated heat flux and heat transfer coefficient. The general form of the uncertainty propagation is expressed as:

$$WR = \left[\left(\frac{\partial R}{\partial X_1}\cdot WX_1\right)^2 + \left(\frac{\partial R}{\partial X_2}\cdot WX_2\right)^2 + \ldots + \left(\frac{\partial R}{\partial X_n}\cdot WX_n\right)^2\right]^{\frac{1}{2}} \quad (4)$$

where R is the calculated quantity, $X_i$ represents the independent measured variables, and WXi is the uncertainty associated with each independent variable. The uncertainties associated with voltage, surface temperature, diameter, and current measurements were considered in the calculation. Under the maximum heat flux condition, the relative uncertainty for heat flux and pool boiling HTC was approximately 8%.

## 2.5. Surface characterization and descriptor variables

Before the boiling experiments, the coated and uncoated surfaces were characterized in terms of structural morphology, roughness, wettability, and coating phase confirmation. SEM analyses were performed to examine the surface morphology of bare and Ni-coated samples. The bare surfaces showed relatively smooth morphology, whereas the Ni-coated surfaces exhibited micro/nano-scale porous structures and cavities. With increasing Ni concentration, the porous structure became more pronounced, and the surface morphology changed from compact fine-grained structures toward larger and more clustered porous features. These cavities were considered potential active nucleation sites during pool boiling.

Surface roughness was measured using a Bruker Contour GT optical profilometer over an area of 0.95 × 1.26 mm. Static contact angle measurements were performed using the sessile drop method with a CAM-101 optical contact angle analyzer. In addition, XRD analyses were conducted using Cu-Kα radiation to confirm the presence of Ni on the coated surfaces. The roughness and contact angle values were then used as surface descriptor variables in the machine learning dataset.

## 2.6. Dataset size, group structure and representativeness

The machine learning dataset was organized according to the experimental matrix of the present study. The dataset consisted of twelve material–surface groups, formed by three substrate materials (Cu, AISI 304 stainless steel, and Al 6061) and four surface conditions for each substrate, namely bare, K1, K2, and K3. This grouping structure reflects the physical organization of the pool boiling experiments, because the data points belonging to the same material–surface combination were obtained from the same boiling curve through successive power increments.

For each group, the point-wise experimental variables included wall superheat, heat flux, and heat transfer coefficient values obtained at different heat-flux levels. In addition to these point-wise variables, surface-level descriptors such as Ni concentration, average surface roughness, and static contact angle were assigned to the corresponding material–surface group. Therefore, each row in the dataset represents a local operating point on a boiling curve, while the group identifier represents the surface on which that point was experimentally measured.

This group-based structure is important for model validation. Since data points obtained from the same boiling curve are physically correlated and cannot be considered fully independent random samples, random train–test splitting may lead to overly optimistic performance estimates. For this reason, the revised analysis used group-based cross-validation, in which complete material–surface groups were kept together during model training and testing. In this way, the model evaluation was designed to test whether the learned relationships could be transferred from one surface group to another, rather than merely interpolating between neighboring points of the same boiling curve.

It should also be noted that the dataset represents a controlled experimental matrix rather than a large open database. Therefore, the machine learning results are interpreted as internal, group-wise predictive performance for the present experimental conditions. Broad generalization to different fluids, pressures, coating thicknesses, or surface morphologies is not claimed. Instead, the purpose of the model is to support the interpretation of the present n-pentane pool boiling experiments by linking the measured thermal response to physically meaningful descriptors such as material type, Ni concentration, roughness, and wettability.

## 2.7. Determination of ONB and operational CHF points

Two fundamental event parameters were considered to represent the initiation and boundary behavior of the boiling process: ONB and CHF. ONB values were read from an independent Excel file, and the given ONB surface temperature for each material-surface group was converted to ONB superheat by subtracting it from the saturation temperature:

$$\Delta T_{ONB} = T_{s,ONB} - T_{sat} \quad (5)$$

In the algorithm, the ONB point is matched with the experimental row closest to the $\Delta T_{ONB}$ value within the relevant experimental group. This approach ensures that ONB values are represented consistently with discrete measurement points in the experimental dataset.

In the revised analysis, CHF was treated as an operationally determined critical heat flux rather than simply as the last recorded data point of each boiling curve. During the experiments, the CHF condition was identified by the formation of a vapor layer between the heating surface and

the liquid, followed by a rapid increase in the surface temperature. When this sudden temperature rise was observed, the power supplied to the heater was immediately cut off and the test was terminated. Therefore, the CHF value used in the present dataset corresponds to the maximum experimentally recorded stable heat flux immediately preceding the observed boiling crisis.

Accordingly, the operational CHF was defined as:

$$q''_{CHF,op} = max(q''_{stable}) \quad (6)$$

where $q''_{CHF,op}$ represents the operational CHF and $q''_{stable}$ denotes the stable heat flux values recorded before the rapid surface-temperature rise. This definition is consistent with the experimental safety procedure used in the present study and avoids overclaiming that post-CHF behavior was fully characterized.

Considering CHF together with surface properties is emphasized as an important requirement in the literature. In current evaluation studies on CHF estimation, it is stated that different methods are used, from traditional experimental correlations to numerical models and machine learning-based approaches, but the generalization ability of singular correlations remains limited due to the multi-parameter nature of CHF [7]. Therefore, in the present study, analyzing CHF not only as an outcome parameter but also in relation to surface roughness, contact angle and coating concentration shows that the study is consistent with the multivariate evaluation trend in the literature.

## 2.8. Data preprocessing and outlier checking

Experimental data were read directly in Excel format; each sheet was matched with its corresponding base material. The data reading algorithm was designed to be flexible to accommodate variations in symbols and spellings in column names. Additional variables such as material name, surface type, Ni concentration, Ra, contact angle, and group ID were added to the dataset. Pressure and saturation temperature were not used as machine learning input variables in the revised model because all experiments were performed under the same local pressure of approximately 0.83 bar and the corresponding saturation temperature of n-pentane was constant at approximately 29 °C. These quantities were used only for defining the experimental condition and calculating wall superheat.

In experimental boiling data, outliers can occur due to measurement noise, transition regime oscillations, temperature reading uncertainties, and local surface heterogeneities. Therefore, outlier checking was performed before modeling. The interquartile range, or IQR method, was used as the default method in the code. Within each material-surface group, the lower and upper limits for the variables ΔT, q", and h are defined as follows:

$$IQR = Q_3 - Q_1 T_{sat} \quad (7)$$

$$X_{\text{lower}} = Q_1 - 1.5\, IQR T_{sat} \quad (8)$$

$$X_{\text{upper}} = Q_3 + 1.5\, IQR T_{sat} \quad (9)$$

Here, $Q_1$ and $Q_3$ represent the first and third quartile values, respectively. Points outside these limits are marked as outliers. However, since the ONB and CHF points are physically significant transition or boundary points, their preservation in the algorithm was preferred. This decision is based on the understanding that outliers in boiling data should not always be considered statistical errors.

This data cleaning strategy is important in two respects. First, it reduces the negative impact of noisy or physically invalid measurements on machine learning models. Second, by preserving physically critical regime change points such as ONB and CHF, it prevents the model from completely losing touch with extreme behaviors representing boiling physics. In the literature, the reliability of experimental data-based models in pool boiling modeling studies is directly related to data quality and the selection of physically significant input variables. While data preprocessing in machine learning-based CHF and HTC prediction studies provides a more flexible structure compared to correlation-based approaches, it is particularly emphasized that physical validity checks must be maintained [7].

## 2.9. Model inputs, target variables, and regression algorithms

In this study, separate regression models were developed for two different target variables: heat flux and heat transfer coefficient. The basic input variables used for heat flux estimation are:

$$X_q = \{\Delta T, material, surface, C_{Ni}, R_a, \theta, P, T_{sat}\} \quad (10)$$

For heat flux prediction, the input vector was defined using the experimentally measured wall superheat and surface-level descriptors:

$$Xq = [\Delta T, material, surface, Ni\ concentration, Ra, \theta] \quad (11)$$

For heat transfer coefficient prediction, the revised model structure was arranged to avoid direct information leakage from the defining equation h = q″/ΔT. Therefore, q″ was not used as an input variable in the primary h-prediction model. The input vector for the primary h model was defined as:

$$Xh = [\Delta T, material, surface, Ni\ concentration, Ra, \theta] \quad (12)$$

This structure allows the model to estimate h using wall superheat and surface descriptors rather than using q″, which is already mathematically embedded in the definition of h. In this way, the predictive performance of the h model is interpreted more conservatively and is not attributed to a direct tautological relationship between q″, ΔT, and h.

In addition, a secondary consistency-oriented h model including q″ may be reported separately, only to show the effect of the direct h = q″/ΔT relationship on model performance:

$$Xh_{,with-q} = [\Delta T, q'', material, surface, Ni\ concentration, Ra, \theta] \quad (13)$$

However, the model without q″ is considered the primary predictive model in the revised manuscript, whereas the model with q″ is discussed only as a derived-variable consistency case.

Three different regression algorithms were selected for model comparison: Random Forest Regressor, Gradient Boosting Regressor, and SVR. Using these three models

together allows for the comparison of different learning characteristics. Random Forest is an ensemble-based method that can capture nonlinear relationships and variable interactions by averaging a large number of decision trees. Gradient Boosting focuses on reducing prior errors through successive trees and can demonstrate strong prediction performance, especially on limited datasets. SVR, on the other hand, is a scale-sensitive method that can represent nonlinear relationships in a high-dimensional space using kernel functions.

The categorical and numerical preprocessing steps were implemented using a pipeline structure. Material type and surface type were treated as categorical descriptors and encoded using one-hot encoding with unknown-category handling. For Random Forest and Gradient Boosting models, encoded categorical variables were combined with the numerical variables, which were passed through without scaling because tree-based models are not sensitive to feature scale. For SVR, the same categorical encoding was used, while numerical variables were standardized using StandardScaler because SVR is sensitive to the relative scale of input variables. Model performance was evaluated using GroupKFold cross-validation, in which each material–surface combination was treated as a group (see Table 2).

Table 2 Hyperparameter settings and preprocessing strategy used for the machine learning models.

| Model | Main hyperparameters | Categorical variable coding | Numerical preprocessing | Validation strategy |
|---|---|---|---|---|
| Random Forest Regressor | n_estimators = 200; min_samples_leaf = 2; random_state = 42; n_jobs = −1 | Material and Surface were encoded using one-hot encoding; unknown categories were ignored. | Numerical variables were passed through without scaling | GroupKFold cross-validation based on Group_ID |
| Gradient Boosting Regressor | n_estimators = 150; learning_rate = 0.03; max_depth = 3; random_state = 42 | Material and Surface were encoded using one-hot encoding; unknown categories were ignored. | Numerical variables were passed through without scaling | GroupKFold cross-validation based on Group_ID |
| Support Vector Regression | kernel = "rbf"; C = 20.0; gamma = "scale"; epsilon = 0.05 | Material and Surface were encoded using one-hot encoding; unknown categories were ignored. | Numerical variables were standardized using StandardScaler | GroupKFold cross-validation based on Group_ID |

The use of machine learning models in pool boiling and CHF literature has increased in recent years. For example, in studies comparing models such as SVR, Random Forest, and artificial neural networks for CHF estimation, it has been shown that data-based methods can capture complex multiparameter relationships more successfully than classical correlations [8]. In addition, it has been reported that machine learning models can be used to reveal nonlinear relationships between surface properties and HTC in associating the pool boiling heat transfer coefficient with surface morphology [9]. In this context, the selection of RF, Gradient Boosting, and SVR models in the present study is both consistent with similar data-based approaches used in the literature and provides a suitable comparison framework considering the size of the experimental dataset and the heterogeneous surface structure.

## 2.10. Model validation, error metrics, and evaluation of prediction performance

Model performance was evaluated using group-based cross-validation instead of random data splitting. The GroupKFold method was used in the code, and each material-surface combination was defined as a group. This approach was preferred to reduce overly optimistic performance prediction that might arise from having very similar experimental points on the same surface together in both the training and test sets.

Group-based validation is particularly suitable for this study because the experimental data points are not entirely independent random samples; points belonging to the same material and surface lie on the same boiling curve and are physically interconnected. Therefore, classical random cross-validation can lead the model to essentially memorize the same surface behavior. The use of GroupKFold, however, tests the generalizability of the model to different surface groups in a more realistic way.

Model success was evaluated using four key statistical metrics: coefficient of determination ($R^2$), mean absolute error (MAE), root mean square error (RMSE), and mean absolute percentage error (MAPE). These metrics are defined as follows:

$$MAE = \frac{1}{n}\sum_{i=1}^{n} | y_i - \hat{y}_i | \, T_{sat} \tag{14}$$

$$RMSE = \sqrt{\frac{1}{n}\sum_{i=1}^{n}(y_i - \hat{y}_i)^2}\, T_{sat} \tag{15}$$

$$MAPE = \frac{100}{n}\sum_{i=1}^{n} \left| \frac{y_i - \hat{y}_i}{y_i} \right| T_{sat} \tag{16}$$

$$R^2 = 1 - \frac{\sum_{i=1}^{n}(y_i - \hat{y}_i)^2}{\sum_{i=1}^{n}(y_i - \bar{y})^2} T_{sat} \tag{17}$$

Here $y_i$ experimental value, $\hat{y}_i$ the value predicted by the model, $\bar{y}$ represents the average of the experimental values, and *n* represents the sample size. The best model selection was made primarily based on the highest $R^2$ value and secondarily on the lowest RMSE value. In the code, this selection was performed separately for both the target variables q" and h.

In the revised analysis, the h-prediction model was interpreted using two different input structures. The primary h model excluded q″ from the input space to avoid direct information leakage from the defining equation h = q″/ΔT. The previously reported q″-included h model was retained only as a secondary consistency-oriented case. Therefore, the high performance of the q″-included model should not be interpreted as independent predictive capacity, but rather as a consequence of the direct mathematical relationship between q″, ΔT, and h.

For q″ estimation, the Gradient Boosting model provided the best performance among the tested algorithms, with $R^2$ = 0.744, RMSE = 64.496 kW/m², MAE = 45.301 kW/m², and MAPE = 49.41%. However, the high MAPE value indicates limited practical accuracy, particularly in low heat-flux and transition regions. Therefore, the q″ model is presented as the best-performing model within the tested set, rather than as a fully optimized predictive tool.

### 2.11. Comparison, residual analysis, and model interpretability

The aim was to evaluate model performance not only with numerical error metrics but also with graphical validation tools. In this context, experimental and predicted values were compared on a 1:1 line, and a linear trend line and 95% confidence interval were added. Thus, it was possible to visually examine whether the model predictions systematically showed a high or low prediction trend. In the code, the 1:1 line, fit curve, and confidence interval are presented on the same graph; the $R^2$, RMSE, MAE, and MAPE values of the relevant model are added to each graph.

The residual values are defined as follows:

$$e_i = \hat{y}_i - y_i \tag{18}$$

In the residual graphs, the random distribution of the values $e_i$ around the zero line indicates that the model does not produce a systematic bias. The resulting graphs show that the residuals for h are generally clustered within a narrow range, but negative deviations become more pronounced in some regions with high heat transfer coefficients. This can be explained by the fact that nonlinear physical effects such as bubble coalescence, dry zone formation, and local surface wettability become more dominant in regions with high heat flux and those approaching CHF. In this prediction, the wider distribution of residues is due to the heat flux exhibiting sharper regime changes along the boiling curve.

Permutation significance analysis was applied to the interpretability of the model. For the best-selected model in the code, the contribution of each input variable to the prediction performance was calculated based on the decrease in the model score when the variable values were mixed. According to the resulting graphs, the most important variable in h prediction is q". This was followed by ΔT. This result is physically expected because the heat transfer coefficient is directly defined by heat flux and surface superheating. In the prediction q", ΔT was the most dominant variable, while material type and surface properties provided secondary contributions. This finding indicates that the principal axis of the boiling curve is surface overheating, but coating and material effects are decisive on the slope of the curve, ONB position, and CHF level.

### 2.12. Methodological rationale and scope of the selected approach

The methodological approach adopted in this study was designed to combine experimental pool boiling analysis with machine learning-assisted interpretation. Pool boiling performance is governed by the coupled effects of wall superheat, surface roughness, wettability, coating morphology, substrate material, and operating condition. Therefore, classical empirical correlations may provide useful reference trends, but they may be limited when different substrate materials and electrochemically modified surfaces are evaluated within the same dataset.

In this context, the present model structure was not based only on point-wise boiling variables. Surface-level descriptors, including Ni concentration, average surface roughness, and static contact angle, were included together with wall superheat and material/surface identifiers. This structure allows the model to relate the measured thermal response to physically meaningful surface parameters rather than treating the boiling data as purely numerical curve-fitting points.

The use of group-based validation is also methodologically important. Since the data points belonging to the same material–surface condition is obtained from the same boiling curve, they are physically correlated. Therefore, random data splitting may lead to overly optimistic model performance. In the revised analysis, complete material–surface groups were considered during validation to provide a more conservative assessment of model behavior across different surface conditions.

It should be emphasized that the objective of the machine learning analysis is not to propose a universal boiling correlation. The dataset represents a controlled experimental matrix for n-pentane pool boiling on bare and Ni-coated Cu, SS, and Al surfaces. Therefore, the model results should be interpreted as dataset-specific, group-wise predictive performance under the present experimental conditions. Broader generalization to other fluids, pressures, coating thicknesses, or surface architectures requires additional external validation and larger datasets.

## 3. Results and Discussion

This section discusses the heat flux, wall superheat, heat transfer coefficient, critical heat flux, and boiling onset findings obtained from n-pentane pool boiling experiments, along with surface characterization and data-driven modeling results. For reader readability, the graphs have been rearranged to show data processing and variable relationships first, then experimental boiling behavior, surface effects, and finally the validation output of the AI models. This ordering reinforces not only the visual flow of the graphs but also the physical cause-and-effect relationship of the experimental mechanism: surface and coating conditions alter the boiling curves and heat transfer coefficient; this alteration is reflected in the ONB and CHF behavior; and the same set of variables determines the predictive success of the machine learning models.

In boiling heat transfer, h is generally defined by the relationship h = q"/ΔT. Therefore, a leftward shift in the q"-

ΔT curves indicates that the same heat flux can be achieved with lower wall superheating; while an increase in the h-q" curves indicates more efficient energy transfer at the same heat flux level. Since CHF represents the safe upper limit of the nucleate boiling regime, the coating's ability to not only increase the h value but also delay the CHF is a fundamental criterion determining the engineering value of the surface design.

## 3.1. Data preprocessing and the general relationship structure between variables

Figure 1.a shows the distribution between the raw data and the cleaned dataset. It is observed that the clean data distribution preserves the main boiling tendencies in the q"-ΔT space, while reducing the extreme points that deviate from the physical curve. This process is particularly important in machine learning models to prevent excessively deviated measurements from disrupting the decision limit. However, sudden jumps in boiling experiments do not always indicate measurement error; point deviations can also occur due to physical reasons such as changes in active nucleation density, transient dry spot formation, local vapor cloak on the surface, or coating heterogeneity.

The correlation map in Figure 1.b summarizes the linear trends in the dataset. The strong positive correlation between ΔT and q" reflects the expected thermal response of pool boiling. The positive relationship between h and q" is also consistent with increased bubble formation frequency and microconvection in the nucleate boiling region. The moderately positive correlation of CHF with q" suggests that the curves diverge in the high heat flux regime upon reaching the critical point. In contrast, the weak or sample-dependent relationship between contact angle and CHF indicates that wettability alone is not a determinant; it should be evaluated together with roughness, porosity, coating integrity, effective nucleation site density and liquid feeding capacity. This finding is consistent with the “single-parameter explanation inadequacy” frequently emphasized in the literature for coated boiling surfaces [4].

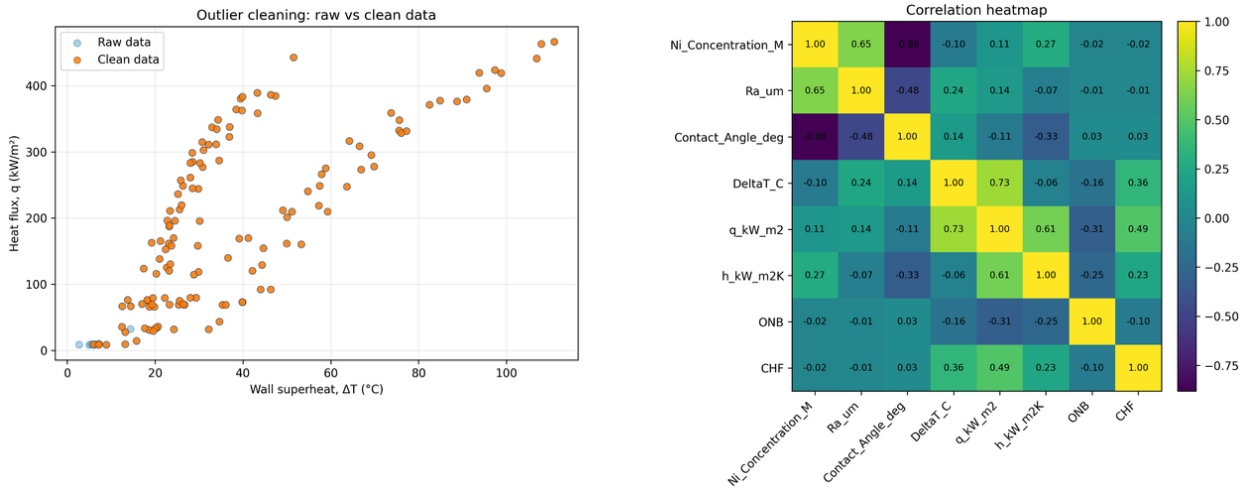


(a) (b)

Figure 1 Preprocessing and correlation structure of the experimental dataset: (a) q"-ΔT distribution after outlier removal, (b) correlation map between model inputs and target variables.

## 3.2. Boiling curves and critical heat flux behavior

Hereafter, CHF refers to the operational CHF defined as the maximum stable heat flux recorded immediately before the observed boiling crisis. Figure 2.a-Figure 2.c show the boiling curves obtained for n-pentane on pure and Ni-coated aluminum, copper, and stainless-steel surfaces. The general trend is a leftward shift of the curve on most coated surfaces, and the same heat flux is achieved at a lower wall superheat. This indicates that the Ni coating creates additional nucleation centers on the difference between coated and pure surfaces is particularly noticeable in aluminum; pure aluminum requires a much higher ΔT to achieve high q" values, while the heat flux in coated aluminum samples increases rapidly over a lower superheating range.

The coating effect on copper surfaces appears more complex. The high thermal conductivity of pure copper can provide an advantage in stabilizing the surface temperature distribution in the low-to-medium heat flux region; however, the CHF level increases, especially in the high heat flux region, with the increase in nucleation centers after coating. Some local fluctuations in the copper curves indicate experimental transition regimes or point data irregularities. Therefore, the number of repeat experiments and uncertainty bands are particularly important for copper samples.

On stainless steel surfaces, CHF values are in the highest range within the entire group. This result cannot be explained solely by the thermal conductivity of the material; because stainless steel has lower thermal conductivity than copper. Here, surface morphology, liquid retention capacity of the coating, microstructure-derived capillary feeding and wettability may be effective together. In the literature, the increase in CHF is often associated with strengthening of liquid refeeding, delay of dry areas and more stable vapor removal pathways [10].

Figure 2.d shows that the most significant improvement in CHF occurs in aluminum and copper after coating, while in stainless steel, the pure surface already starts at a high CHF level and shows further increase with coating. From the graphs, it can be seen that in aluminum, the pure surface increased from approximately 358 kW/m² to 443 kW/m²

after coating; in copper, the pure surface increased from approximately 287 kW/m² to the 380-390 kW/m² range in coated surfaces; and in stainless steel, it reached around 465 kW/m² from approximately 420 kW/m².

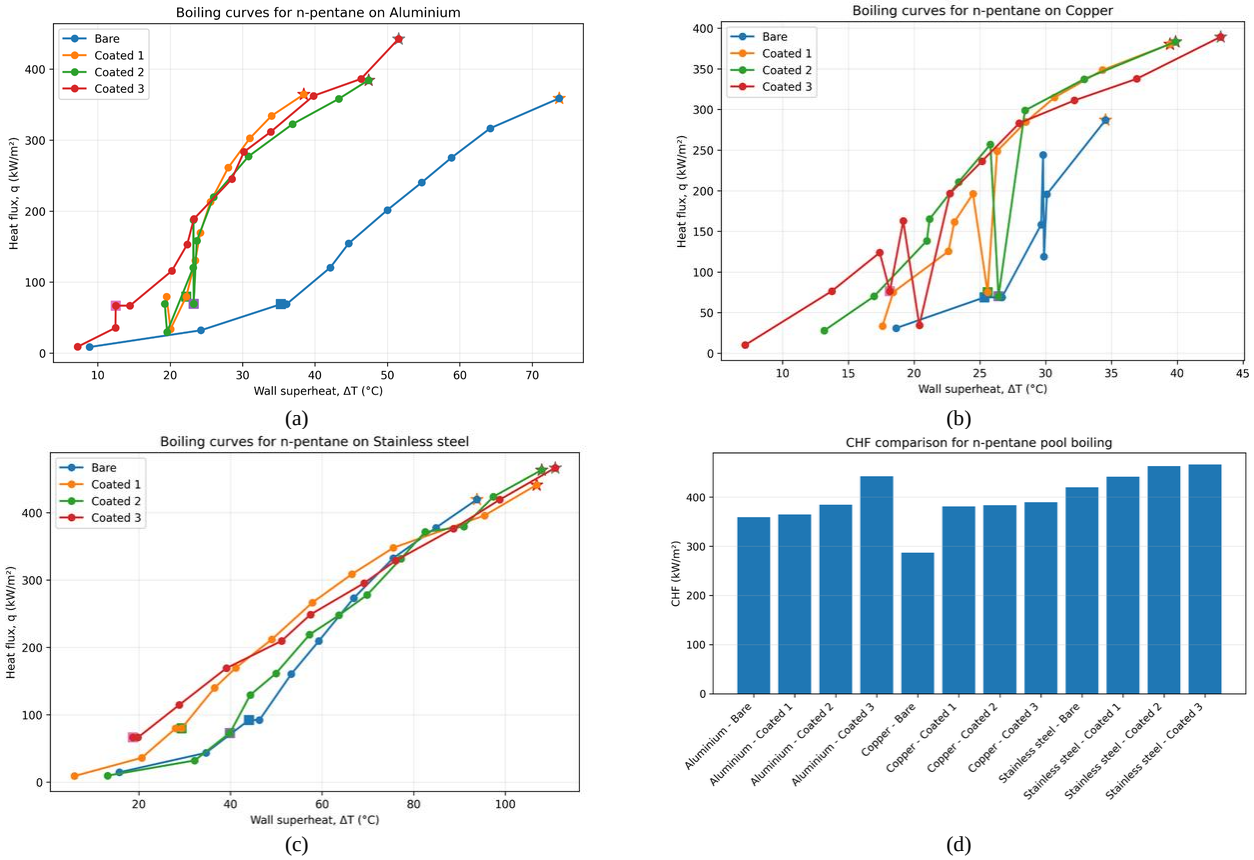


Figure 2 Comparison of experimental boiling curves and CHF in n-pentane pool boiling: (a) aluminum, (b) copper, (c) stainless steel, (d) operational CHF values for all samples.

## 3.3. Heat transfer coefficient curves

Figure 3 shows the variation of the heat transfer coefficient with heat flux in different substrate materials. In aluminum, the h value of the pure surface shows a limited increase with increasing q", while coated surfaces exhibit increases of approximately twofold. The fact that the h curves in coated aluminum samples approach the level of 9-10 kW/m²K in the mid-to-high q" region suggests that the nucleation density and bubble-induced mixing are significantly improved compared to the pure surface. This result is consistent with studies showing that pure metal surfaces with low surface energy or low effective nucleation site can be activated by coating [3].

In copper, h values generally remain in the high range for all samples. While pure copper samples reach levels of 8-9 kW/m²K, h values on coated surfaces reach around 10 kW/m²K. Here, the coating effect is relatively more limited compared to aluminum, but the improvement is more stable. This can be explained by the fact that copper, thanks to its high thermal diffusibility, maintains a more homogeneous substrate temperature, and the Ni coating provides additional nucleation contribution. However, it should also be considered that the conduction resistance between the substrate and the liquid may increase when the thickness of the coating layer is large.

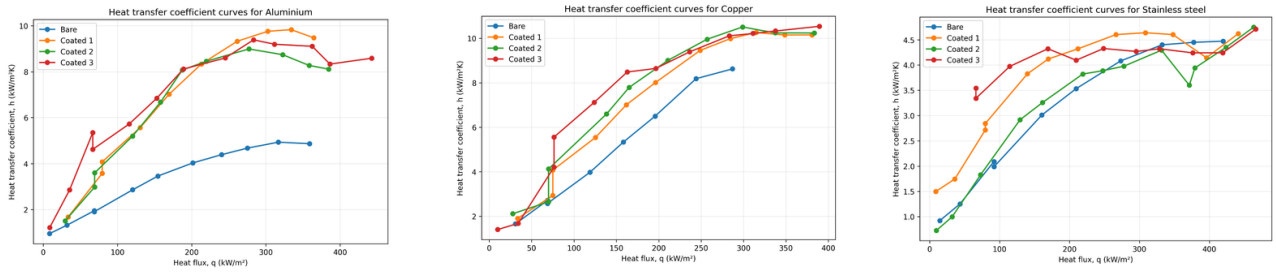


Figure 3 Heat transfer coefficient curves for pure and Ni-coated surfaces: (a) aluminum, (b) copper, (c) stainless steel.

In stainless steel, h values appear to be in a lower range compared to the other two materials; however, an earlier rise after coating and convergence in the high q" region are observed compared to the pure surface. This indicates that although stainless steel exhibits high performance in terms of CHF, its instantaneous h values may not be as high as those of copper and coated aluminum. Therefore, the “highest h” and the “highest CHF” may not necessarily

coincide on the same surface. This distinction can alter surface selection in pool boiling design, depending on whether the goal is high heat transfer with low superheat or a safe maximum heat flux.

### 3.4. Ni concentration, ONB and boiling onset

Figure 4.a shows that CHF generally increases as the Ni coating concentration increases. The upward trend is most uniform in stainless steel, while a sharper increase is observed in aluminum at high concentration levels. In copper, although there is a large jump in the transition from pure to coated surfaces, the effect of subsequent concentration increases is more limited. This result suggests that the coating significantly alters the effective nucleation centers and surface wettability in the initial stage; however, after a certain density, the increase in CHF may approach saturation.

(a)

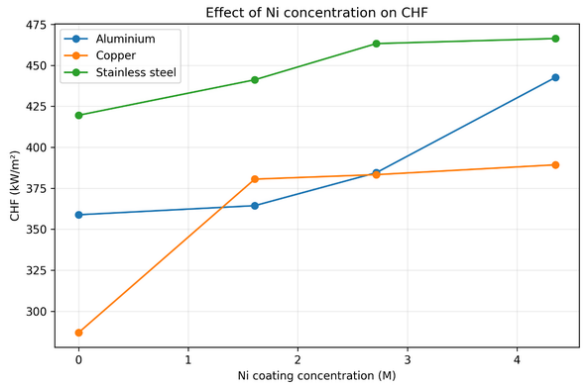


(b)

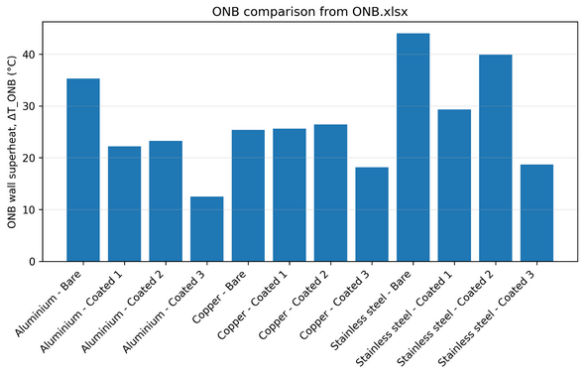


Figure 4 Effect of Ni coating concentration on critical heat flux and ONB comparison: (a) CHF-Ni concentration relationship, (b) ONB values according to samples.

When the ONB values are examined in Figure 4.b, it is seen that some coated samples significantly reduce the onset of boiling to a lower wall superheat. The third coated aluminum sample has a significant advantage over the pure surface with an ONB value of approximately 12-13°C. The ONB value of the third coated copper sample is also lower than that of the pure surface and other coated samples. In stainless steel, while the ONB of the pure surface appears high, the onset of boiling is significantly improved with coating, especially in some samples. Lower ONB indicates earlier activation of stable vapor nuclei on the surface and is therefore valuable for compact heat exchanger designs operating with low temperature differences.

However, a decrease in ONB does not always mean that CHF will increase proportionally. While ONB is sensitive to the initiation of nucleation; CHF is associated with liquid feeding, vapor removal and dry area formation in the high heat flux region. Therefore, ONB and CHF should be discussed together, and the coating's capacity to not only initiate early boiling but also feed the surface with liquid at high heat load should be evaluated. This distinction is consistent with the general acceptance in the literature that the nucleation and CHF mechanisms have different control parameters [11].

### 3.5. Surface roughness and wettability effects

Figure 5.a shows that there is a generally positive trend between surface roughness and CHF, but this relationship is distributed depending on the material and coating type. High roughness or suitable coating morphology is seen in stainless steel with high CHF, while significant improvements are also obtained at medium roughness levels in copper and aluminum. This result shows that roughness can be beneficial on h and ONB because it increases the number of nucleation voids; however, it is not sufficient on its own for CHF. Very high roughness can be beneficial if the pores facilitate liquid feeding; however, it can also have a counterproductive effect in irregular morphologies that prevent vapor from escaping the surface [12].

Figure 5.b shows that the distribution between Ra and h does not form a distinct linear relationship. This indicates that the value of h depends not only on surface roughness but also on the working point. This indicates that it is affected by multiple variables such as wall heat, substrate material, coating concentration, and wettability. In particular, since h is calculated as q"/ΔT ratio, significantly different h values can occur in different heat flux regions at the same roughness value. Therefore, it is meaningful to include surface roughness as a model input in h estimation; however, it is expected to play a secondary explanatory role alongside direct thermal variables such as ΔT.

Figure 5.c and Figure 5.d show that the effect of contact angle is even more sample-dependent. In general, a lower contact angle means better wettability and can contribute to the increase in CHF. However, the graph shows samples with different CHF values despite having a low contact angle, and divergent behaviors in the high contact angle region. This table supports the need to evaluate the wettability-capillary feed-microstructure triad together, as emphasized in the literature [13]. If the contact angle is taken by static measurement, the dynamic wettability of the surface during boiling and the temperature-dependent liquid-surface interaction should also be considered.

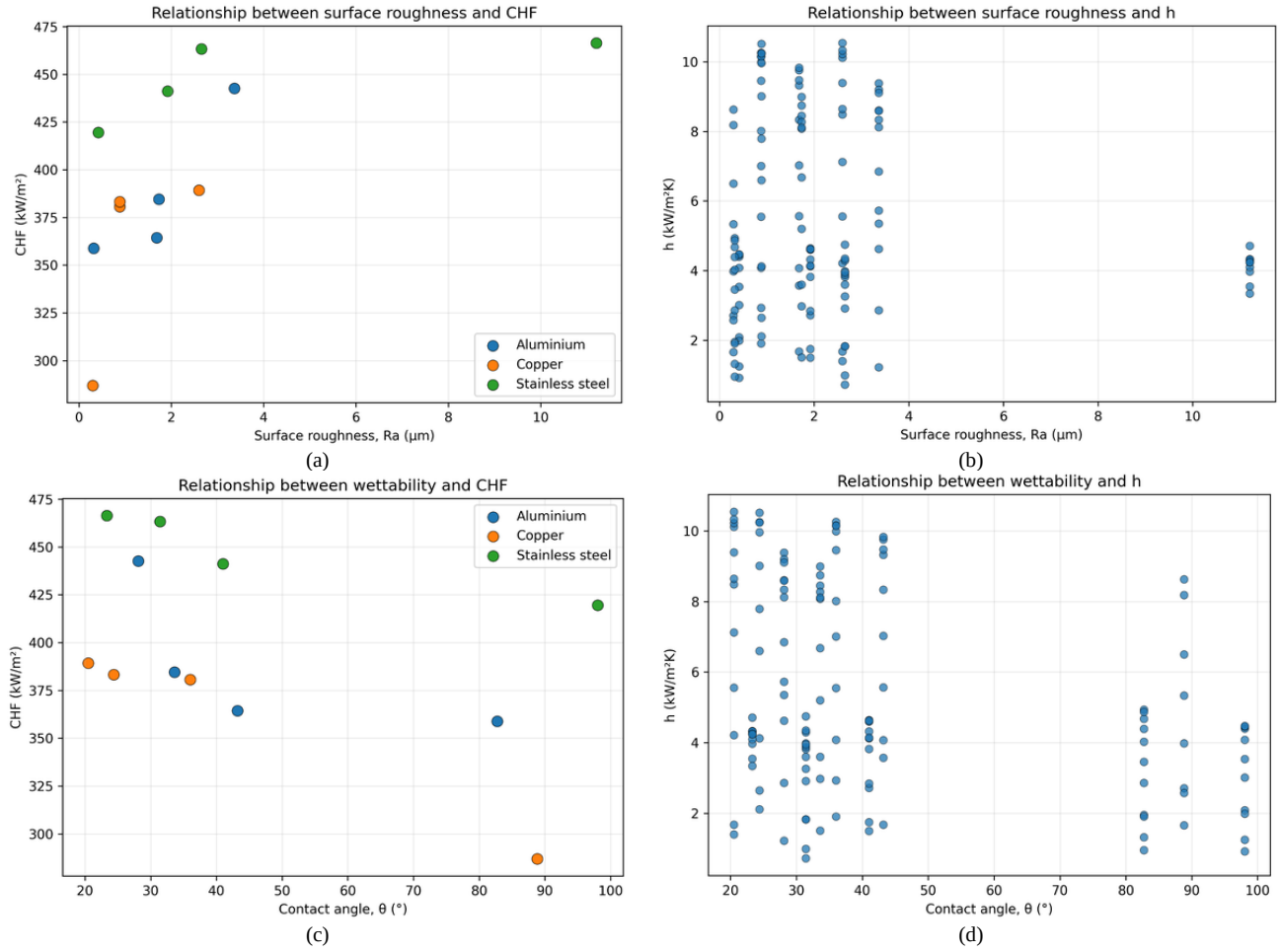


Figure 5 Relationships between surface characterization parameters and boiling performance: (a) Ra-CHF, (b) Ra-h, (c) contact angle-CHF, (d) contact angle-h.

## 3.6. Comparative evaluation of artificial intelligence models

The h-prediction results shown here correspond to the q″-included secondary consistency model and are therefore interpreted with caution. The primary q″-excluded h model is required for independent predictive assessment. Figure 6 compares the performance of SVR, Gradient Boosting, and Random Forest models for heat transfer coefficient and heat flux estimation. Within the q″-included secondary consistency case, the SVR model provided the highest apparent performance in estimating h. The graph shows $R^2$=0.921, RMSE=0.801, MAE=0.55, and MAPE=14.08% for SVR. This performance can be explained by the fact that the h variable is strongly defined by direct physical variables such as q" and ΔT in the dataset, and SVR generalizes well to small/medium-sized, nonlinear but regular datasets.

Gradient Boosting and Random Forest models also perform at an acceptable level in h estimation; however, error values are higher and $R^2$ is lower compared to SVR. The possible reason for this may be the limited number of data points and the fact that tree-based models produce generalization errors by adapting more to local fluctuations in the dataset [14].

In q" estimation, the Gradient Boosting model is the most successful option. The graph shows $R^2$=0.744, RMSE=64.496 kW/m², MAE=45.301 kW/m², and MAPE=49.41% for Gradient Boosting. Random Forest gives similar but slightly weaker results, while SVR is significantly inadequate in heat flux estimation. This discrepancy may stem from the fact that the q" variable varies over a wide range and depends on the regimes in the experimental curves. In particular, boiling onset, nucleate boiling development, and the regions approaching CHF may not be fully represented by a single continuous function. The improvement of error regions with successive weak learners by Gradient Boosting appears to have provided an advantage in q" estimation.

Model results are generally consistent with AI-based approaches reported in the literature for boiling heat transfer: higher $R^2$ and lower error values are obtained in targets with strong direct physical connection, while prediction uncertainty increases in regions near regime transitions and critical events [15].

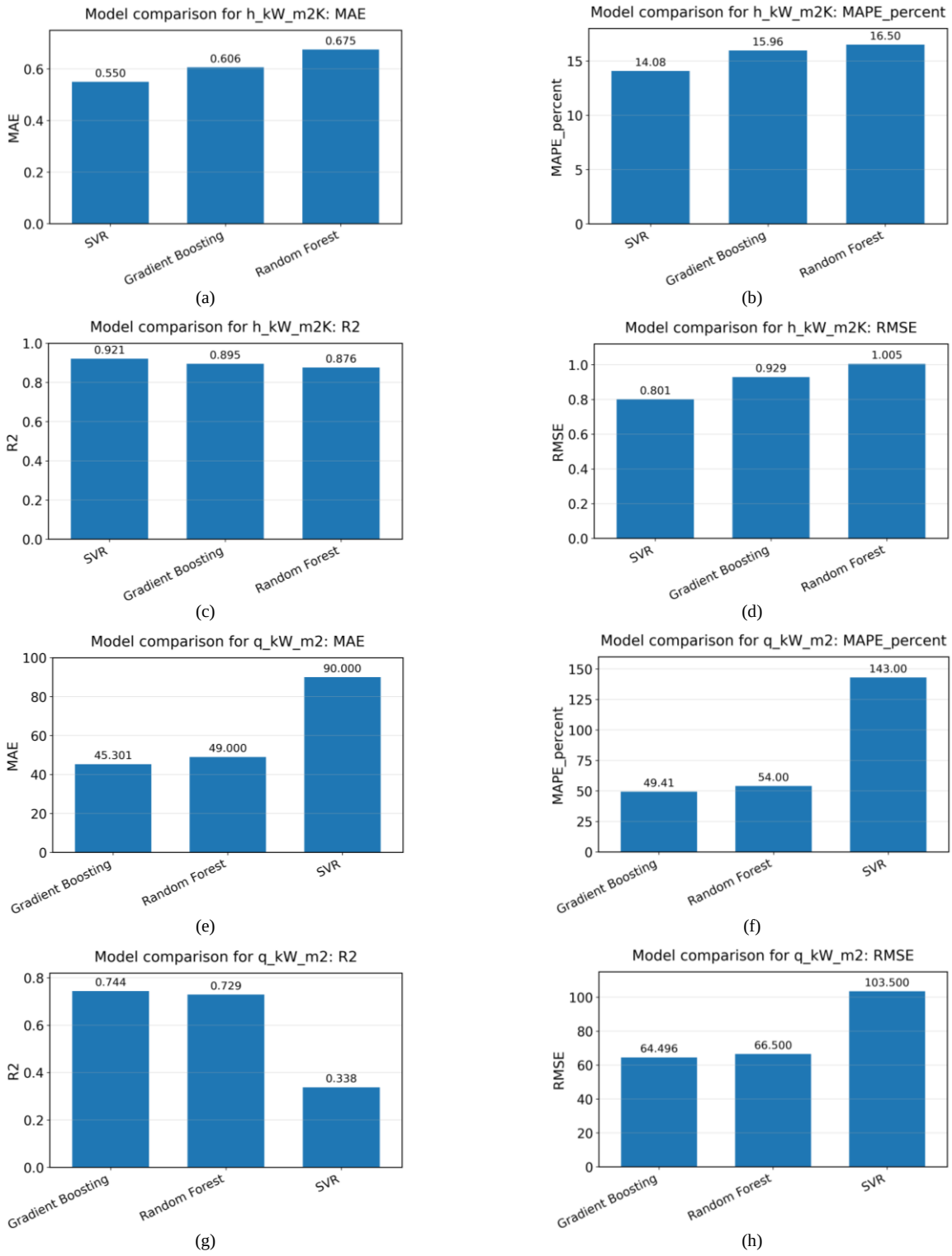


Figure 6 Comparison of machine learning model success metrics for target variables h and q": MAE, MAPE, $R^2$, and RMSE.

## 3.7. Prediction accuracy and residual analysis

Figure 7.a shows that the SVR model's h predictions are quite close to the experimental values. The clustering of points close to the 1:1 line and the narrow confidence interval indicate that the model successfully captures the general trend. However, there are some deviations in the mid and high h regions. These deviations may be due to the fact that different material/coating groups operate with different physical mechanisms within the same h range. Therefore, it is important for the model to consider material and surface properties; however, the effect of these variables can only be learned to a limited extent without increasing the number of data points.

Figure 7.b shows that the Gradient Boosting model follows the general trend for q" estimation, but the scattering is wider compared to h estimation. In particular, some points deviate from the 1:1 line in the low-to-medium heat flux range and the high heat flux region. The high MAPE value in q" estimation may be related to the increase in relative error at small experimental q" values. Therefore, using metrics such

as MAE or normalized RMSE in addition to MAPE for the low q" region may provide a more balanced assessment.

Figure 7.c and Figure 7.e show that in the h model, the residuals are mostly clustered around zero, but there are a few negative end residuals. This suggests that the model underestimates the h value under some conditions, or that there are local mechanisms within the experimental data that the model cannot capture. In Figure 7.d and Figure 7.f, the residuals of the q" model exhibit a wider distribution, with particularly high positive residuals. This indicates that at some high heat flux points, the model produces predictions exceeding the experimental value. This observation is important because overestimation in the high q" region near CHF is risky from a safety perspective.

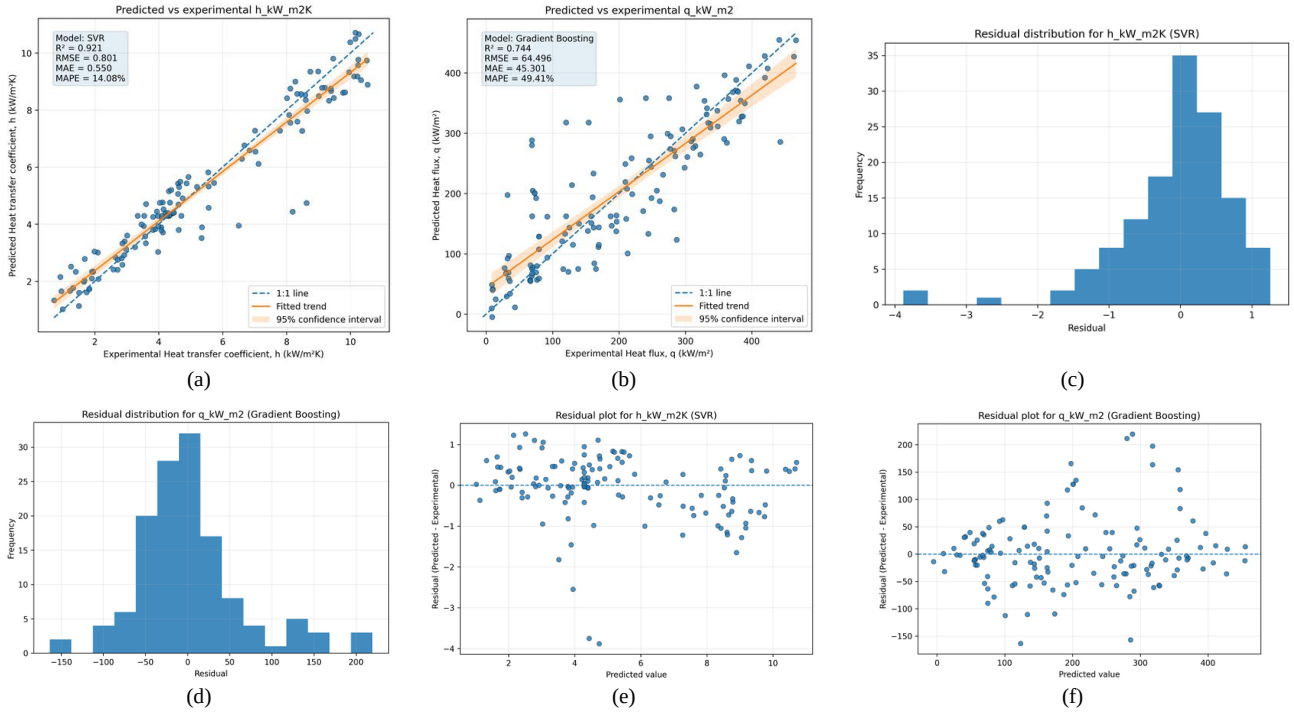


Figure 7 Estimation and residual analyses for the most successful models: (a) experimental-prediction comparison for h, (b) experimental-prediction comparison for q", (c-d) residual distributions, (e-f) residuals versus prediction value plots.

## 3.8. Feature importance and physical interpretation

Figure 8.a shows that heat flux is the most dominant input in the prediction of h. This result is physically expected because, according to the definition of h=q"/ΔT, heat flux is directly involved in the calculation of the h value. The fact that ΔT is in second place is also consistent with the same physical relationship. The lower order of importance of surface parameters such as material, Ra, contact angle, and Ni concentration indicates that instantaneous thermal variables are dominant in the point-by-point prediction of h, while surface properties indirectly shape this thermal response.

Figure 8.b shows that ΔT is the most important variable in predicting q". This is an expected result due to the strong variation of heat flux with wall superheating in boiling curves. The second-ranked material indicates that different substrates can produce different q" values at the same ΔT level. Contact angle, surface type, and Ra and Ni concentrations offer lower but physically significant contributions. This ranking is valuable because it shows that the machine learning model not only produces mathematical fit but also captures a significance structure consistent with fundamental boiling physics. However, caution should be exercised in interpreting feature significance.

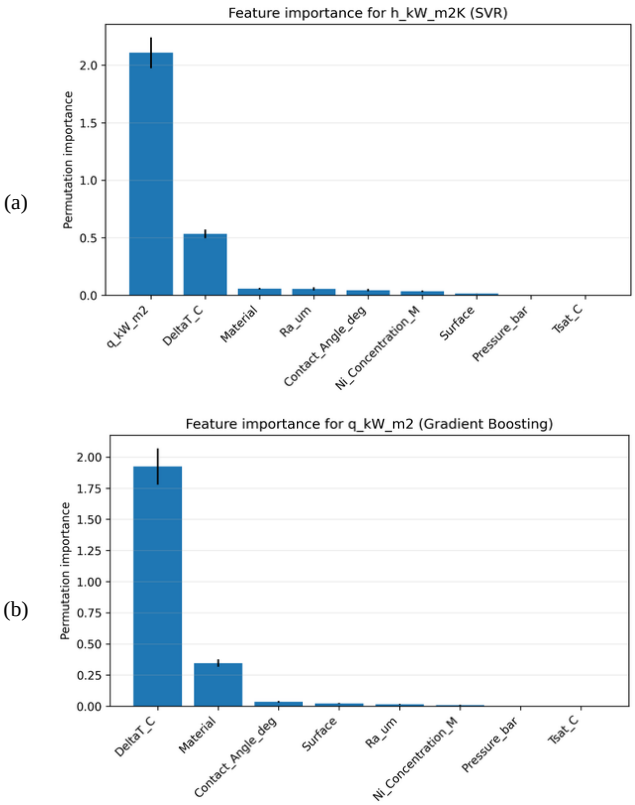


Figure 8 Permutation-based feature significance for the most successful models: (a) SVR for h estimation, (b) Gradient Boosting for estimation.

Using directly related variables such as q" and ΔT in the h model can improve model performance but may lead to discussions about "information leakage" in terms of physical exploration. This approach is suitable if the aim is to predict the h value from q" and ΔT calculated after the experiment; however, if the aim is only to predict performance from surface characterization parameters, q" and ΔT should be evaluated separately as derived/operational variables related to the target. The feature-importance results for h correspond to the q″-included secondary consistency model.

### 3.9. Compatibility with literature and original contribution

The results obtained are consistent with the literature trend that coated and micro/nano-structured surfaces reduce ONB by increasing the nucleation site density in pool boiling, increase the h value in the nucleate boiling region, and increase CHF when a suitable liquid feed/vapor removal balance is achieved [10]. The distinctive aspect of the study is that it evaluates the effect of Ni coating concentration on different substrate materials not only with experimental curves but also with surface roughness, wettability, correlation analysis and artificial intelligence-based prediction models.

The significant increase in h and CHF after coating, particularly in aluminum, demonstrates that low-cost and lightweight substrates can be transformed into high-performance boiling surfaces through surface engineering. In copper, the coating effect is greater in terms of CHF compared to the pure surface, but more limited with subsequent concentration increases, suggesting that optimum coating density is critical in substrates with high thermal conductivity. The high CHF performance in stainless steel is important because it shows that the combination of coating, morphology, and wettability can provide a strong CHF improvement independent of substrate thermal conductivity.

The AI outputs are consistent with the literature in two respects. Firstly, high accuracy was achieved in targets strongly defined by physical formulas such as h. Secondly, model success was more limited in the wide-ranging and regime-transition-sensitive target such as heat flux (q"). This shows that classical regression metrics alone are insufficient for boiling data; approaches such as regime-based modeling, uncertainty analysis, and physics-informed feature selection are necessary [15, 16].

### 3.10. Comparative general assessment

Table 3 summarizes the general trends read from the graphs. In general, Ni coating improved the surface performance in n-pentane pool boiling in a material-dependent manner. The leftward shift of the boiling curves, the decrease in ONB, the increase in h values, and the rise in CHF on coated surfaces indicate that surface engineering can improve both heat transfer density and critical heat load safety. However, the magnitude of the improvement depends on the substrate material, coating concentration, roughness, and wettability; therefore, optimum surface design should be done by evaluating multiple physical parameters together, not just a single parameter.

Table 3 Comparative summary of experimental and modeling results based on graphs.

| Material | The most significant experimental finding | Approximate CHF trend | ONB behavior | Compatibility with literature review. |
|---|---|---|---|---|
| Aluminum | The post-coating boiling curve shifted significantly to the left; h and CHF increased. | Pure ~358 kW/m²; optimal coating ~443 kW/m². | Coating 3 reduces the ONB temperature to ~12-13 °C. | The increased nucleation and earlier onset of boiling after coating are consistent with the literature. |
| Copper | Strong increase in CHF after coating; h values are generally high and stable. | Pure ~287 kW/m²; coated surfaces ~380-390 kW/m². | Coating 3 provides lower ONB than pure and other coatings. | High thermal conductivity + coating-induced increased nucleation is the expected behavior. |
| Stainless steel | The highest CHF range was observed in the stainless steel group. | Pure ~420 kW/m²; coated surfaces ~442-467 kW/m². | Coating significantly reduces ONB in some samples. | The increase in CHF is consistent with fluid supply/capillary action and surface morphology. |
| h prediction model | h prediction model: In the q″-included secondary consistency case, SVR showed the highest apparent performance. | $R^2$=0.921; RMSE=0.801; MAE=0.550; MAPE=14.08%. | Not applicable. | The dominance of q" and ΔT is consistent with the physical description. |
| q" prediction model | Gradient Boosting is the best model; however, the error rate is higher compared to the h-model. | $R^2$=0.744; RMSE=64.496; MAE=45.301; MAPE=49.41%. | Not applicable. | Due to regime transitions, it is more difficult to predict q"; this is an expected situation in the literature. |

Artificial intelligence models have shown that experimental findings can be supported by data. The SVR model yielded high accuracy in h estimation, while the Gradient Boosting model provided the best result in q" estimation. However, the high relative error in q" estimation and the breadth of the residual distribution indicate that boiling regimes and regions near CHF require more detailed modeling. Future studies using larger datasets, uncertainty analysis, explainable artificial intelligence, regime-based modeling, and additional features representing surface morphology will improve predictive power and physical interpretability.

## 4. Conclusion

In this study, the pool boiling behavior of n-pentane fluid on uncoated and nickel-coated copper, aluminum, and stainless-steel surfaces were evaluated using experimental data and a machine learning-supported prediction approach. The effects of substrate material, nickel coating concentration, surface roughness, and wettability were investigated through boiling curves, heat transfer coefficient, ONB, and CHF results. Experimental results showed that nickel coating generally improved boiling performance. However, the level of this improvement varied depending on the surface material and coating condition. On coated aluminum surfaces, boiling started at lower surface superheat values, high heat transfer coefficients were obtained on copper surfaces, and stainless-steel surfaces stood out with the highest CHF values. This indicates that boiling performance is determined not by a single surface parameter, but by the combined effect of surface morphology, wettability, coating concentration, and substrate material. CHF results revealed that increased wettability can delay dry zone formation by promoting fluid rewetting. However, nonlinear trends between roughness, contact angle, and CHF indicate that an optimum surface condition is necessary for peak performance.

In the machine learning results, the heat transfer coefficient h was predicted with higher accuracy than the heat flux q". The SVR model yielded the most successful results in h prediction, while the Gradient Boosting model was most successful in q" prediction. The h-prediction results were interpreted cautiously because h is mathematically related to q″ and ΔT. In the revised model structure, q″ was removed from the primary h-prediction input space to reduce direct information leakage, while the q″-included model was retained only as a secondary consistency case. The higher scattering in q" prediction is due to the strong nonlinear behavior of the boiling curve, especially in the ONB and CHF regions. Variable significance analysis supported the physical consistency of the models. While heat flux and surface superheating were the most influential [11] variables for the heat transfer coefficient, surface superheating was determined to be the dominant variable in heat flux prediction. Furthermore, the use of group-based cross-validation reduced overly optimistic model performance that might result from data belonging to the same boiling curve.

Overall, this study demonstrates that a surface feature-supported machine learning approach offers an effective method for analyzing and predicting the boiling behavior of n-pentane pools. Future studies are recommended to expand the dataset using different coating thicknesses, surface morphologies, operating pressures, and fluids; furthermore, to perform uncertainty analysis and external validation with independent datasets.

## Conflict of Interest

The authors have no conflicts of interest to declare.

## References

[1] Liang G, Mudawar I. Pool boiling critical heat flux (CHF) – Part 2: Assessment of models and correlations. *International Journal of Heat and Mass Transfer* (2018) **117**:1368–1383. doi:10.1016/j.ijheatmasstransfer.2017.09.073.

[2] Zhang Y, Chen G, Du K, Li S, Liu J, Chen F, et al. Review of recent advancing pool boiling heat transfer through surface engineering. *Renewable and Sustainable Energy Reviews* (2026) **230**:116734. doi:10.1016/j.rser.2026.116734.

[3] Liu B, Cao Z, Zhang Y, Wu Z, Pham A, Wang W, et al. Pool boiling heat transfer of N-pentane on micro/nanostructured surfaces. *International Journal of Thermal Sciences* (2018) **130**:386–394. doi:10.1016/j.ijthermalsci.2018.05.012.

[4] O'Hanley H, Coyle C, Buongiorno J, McKrell T, Hu L-W, Rubner M, et al. Separate effects of surface roughness, wettability, and porosity on the boiling critical heat flux. *Applied Physics Letters* (2013) **103**(2):24102. doi:10.1063/1.4813450.

[5] Qi S, Han B, Zhu X, Yang B-W, Xing T, Liu A, et al. Machine learning in critical heat flux studies in nuclear systems: A detailed review. *Progress in Nuclear Energy* (2025) **179**:105535. doi:10.1016/j.pnucene.2024.105535.

[6] Upot NV, Fazle Rabbi K, Khodakarami S, Ho JY, Kohler Mendizabal J, Miljkovic N. Advances in micro and nanoengineered surfaces for enhancing boiling and condensation heat transfer: a review. *Nanoscale advances* (2023) **5**(5):1232–1270. doi:10.1039/d2na00669c.

[7] Li J, Huang Y, Qiu Y, Wang S, Yang Q, Wang K, et al. Prediction of critical heat flux using different methods: A review from empirical correlations to the cutting-edge machine learning. *International Communications in Heat and Mass Transfer* (2025) **160**:108362. doi:10.1016/j.icheatmasstransfer.2024.108362.

[8] Swartz B, Wu L, Zhou Q, Hao Q. Machine learning predictions of critical heat fluxes for pillar-modified surfaces. *International Journal of Heat and Mass Transfer* (2021) **180**:121744. doi:10.1016/j.ijheatmasstransfer.2021.121744.

[9] Ma B, Zhao Z, Sun M, Liu B. Machine learning-based prediction of nucleate pool boiling heat transfer enhancement on micropillar surfaces. *International Communications in Heat and Mass Transfer* (2025) **166**:109116. doi:10.1016/j.icheatmasstransfer.2025.109116.

[10] Liang G, Mudawar I. Review of pool boiling enhancement by surface modification. *International Journal of Heat and Mass Transfer* (2019) **128**:892–933. doi:10.1016/j.ijheatmasstransfer.2018.09.026.

[11] Kandlikar SG. A Theoretical Model to Predict Pool Boiling CHF Incorporating Effects of Contact Angle and Orientation. *Journal of Heat Transfer* (2001) **123**(6):1071–1079. doi:10.1115/1.1409265.

[12] Moghadasi H, Malekian N, Saffari H, Mirza Gheitaghy A, Zhang GQ. Recent Advances in the Critical Heat Flux Amelioration of Pool Boiling Surfaces Using Metal Oxide Nanoparticle Deposition. *Energies* (2020) **13**(15):4026. doi:10.3390/en13154026.

[13] Betz AR, Jenkins J, Kim C-J“, Attinger D. Boiling heat transfer on superhydrophilic, superhydrophobic, and superbiphilic surfaces. *International Journal of Heat and Mass Transfer* (2013) **57**(2):733–741. doi:10.1016/j.ijheatmasstransfer.2012.10.080.

[14] Hastie T. *The elements of statistical learning: Data mining, inference, and prediction*. S.l.: Springer-Verlag (2009). 758 p.

[15] Rashidi MM, Alhuyi Nazari M, Harley C, Momoniat E, Mahariq I, Ali N. Applications of machine learning methods for boiling modeling and prediction: A comprehensive review. *Chemical Thermodynamics and Thermal Analysis* (2022) **8**:100081. doi:10.1016/j.ctta.2022.100081.

[16] Mehdi S, Borumand M, Hwang G. Accurate and robust predictions of pool boiling heat transfer with micro-structured surfaces using probabilistic machine learning models. *International Journal of Heat and Mass Transfer* (2024) **226**:125487. doi:10.1016/j.ijheatmasstransfer.2024.125487.